Challenges, Opportunities and Solutions in Structural Engineering and Construction – Ghafoori (ed.)
© 2010 Taylor & Francis Group, London, ISBN 978-0-415-56809-8

Behavior of cylindrical R/C panel under combined axial and lateral load

T. Hara
Tokuyama College of Technology, Shunan, Japan

ABSTRACT: R/C cylindrical panels have been often used for the storage reservoir, tank, stack and cooling tower structures. They usually possess the high ultimate strength under lateral uniformly distribute loading. Therefore, they are used for the wall structure. However, when R/C cylindrical panels have heavy roof structure such as the underground LNG tanks or they are huge structures such as tall stacks or the huge cooling towers, they are subjected to combined axial compressive and lateral flexural loadings. In this paper, the deformation characteristics and the ultimate strength of R/C cylindrical panel under combined axial and flexural loadings are investigated numerically. In numerical analyses, FEM procedures are used based on the degenerate shell formulation. The numerical parameters are obtained from the experimental results and the numerical models are constructed based on the experimental specimens. The distribute or the concentrate loadings are considered as the flexural loading.

1 INTRODUCTION

R/C cylindrical panels have been often used for the storage reservoir, tank, stack and cooling tower structures. They usually possess the high ultimate strength under lateral uniformly distribute loading. Therefore, they are used for the wall structure in underground or the roof structure. However, when R/C cylindrical panels have heavy roof structure such as the underground LNG tanks or they are huge structures such as tall stacks or the huge cooling towers, they are subjected to combined axial compressive and lateral flexural loadings. From the previous paper (Hara 2008), the comparisons between the numerical and the experimental results concerning R/C cylindrical shell panel under the concentrate or the distribute lateral loading were presented. In the analyses, R/C cylindrical shell were pin-supported on both meridional and hoop edges. Both numerical and experimental results were well agreed. In this paper, the deformation characteristics and the ultimate strength of R/C cylindrical panel subjected to a combined axial and a flexural loadings are investigated numerically under the same geometric and supporting conditions.

R/C panels are made by micro concrete and steel wire meshes. The specimens are 960 mm × 950 mm plan and the thickness of the panel is 10 mm. The span to depth ratio is 5 (see Figure 1). The panels contain a reinforcement mesh sheet in the middle of the shell panel. The reinforcement wire is 0.75 mm diameter and placed with equidistant spacing 5 mm in both meridional and hoop directions. The specimens are supported on both meridional and hoop edges by roller hinges. The deformations are evaluated at each loading step. The ultimate load is obtained by the peak loading on the load deflection curve.

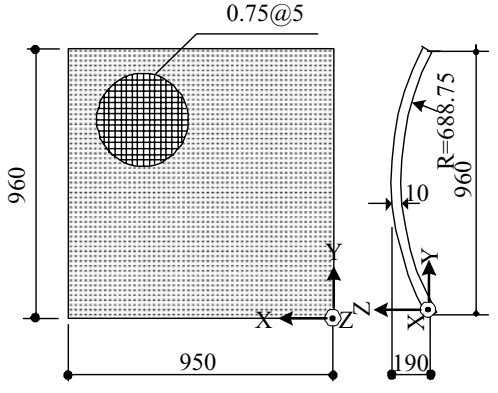

Figure 1. Geometric dimensions of R/C shell (unit: mm).

In numerical analyses, FEM schemes are used based on the degenerate shell formulation. The numerical parameters are obtained from the experimental results and the numerical models are constructed based on the experimental specimens. Load deflection characteristics and the ultimate strength are computed under several combinations of loadings.

2 DEFINITION OF THE SPECIMEN

2.1 *Geometric dimensions*

R/C panel has the cylindrical shape with 960 mm × 960 mm plan and has 688.75 mm radius and 10 mm

thickness (see Figure 1). ϕ0.75 mm stainless wires are used as the reinforcements and are placed in the middle of the shell thickness in both meridional and hoop direction. They are placed in equi-distance 5 mm. The specimen is made by use of the steel mold to avoid the geometric imperfections. The micro concrete with aggregate size 2.5 mm is used. The material properties are shown in Table 1 and 2.

2.2 *Supporting and loading conditions*

Specimens are pin-supported by steel ball-hinges of 11 mm diameter arranged at 20 mm spaces on both meridians. Also, both hoop edges are pin-supported by the same apparatus.

Table 1. Material properties of concrete.

Compressive strength (MPa)	38.2
Tensile strength (MPa)	3.8
Young's modulus (GPa)	23.6
Poisson's ratio	0.20

Table 2. Material properties of steel.

Yield stress (MPa)	235
Tensile stress (MPa)	449
Young's modulus (GPa)	206
Tangential modulus (GPa)	21

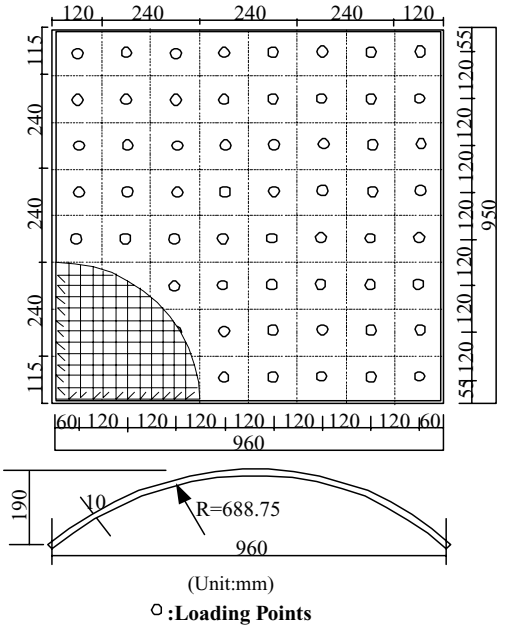

Figure 2. Quasi-uniformly distributed load.

Two types of lateral loading conditions are considered. One is the concentrate load at the center of the shell plane. The other is the quasi-distribute load on the shell plane. The quasi-distribute load is applied as 64 concentrate loads, that are summarized to the one concentrate load via whiffle tree loading system (see Figure 2).

3 NUMERICAL PROCEDURE

3.1 *Numerical model*

In numerical analyses, the finite element procedure is applied. Figure 3 shows the FE mesh of this analysis. The full model is adopted. The model is divided into 32 elements in meridional and hoop directions, respectively. Each element is divided into 8 concrete layers and 2 steel layers. Boundary conditions are pin-supported along both meridional and hoop edges. All rotations are free on all edges.

3.2 *Finite element*

In numerical analysis, the geometric and material nonlinearlities are considered. 9 nodes Heterosis element is used and 2 $\times$ 2 reduced integration is adopted to avoid the numerical problems.

The numerical simulation is performed under the displacement incremental scheme. The yield condition of concrete is defined as the Dracker-Prager type, which is assumed that concrete yields when the equivalent stress based on mean stress and second deviatoric stress invariants reaches uniaxial compressive strength (Hinton 1984). The crushing condition is contorolled by strain. The ultimate compressive strain of concrete is assumed as 0.003 by Kupfer's experiment (Kupfer

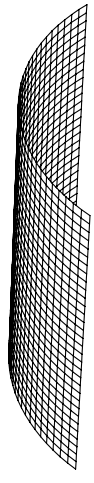

Figure 3. FE Mesh.

1969). Also, after cracking of concrete, the tension stiffenig parameters accounting for the tensile strength of concrete are introduced. The material nonlinearlities of steel are assumed to be bilinear stress-strain relation for the reinforcement.

4 NUMERICAL RESULTS

Two types of lateral loading conditions are considered. One is the concentrate load at shell center. The other is the quasi-uniformly distribute load of the shell plane. After applying the axial force in meridional direction, these two types of lateral loadings are applied, respectively.

4.1 *Fundamental load bearing characteristics*

4.1.1 *R/C shell under axial compression*

Figure 4 represents the relation between an axial load and deformation in the direction perpendicular to the shell plane at the center of the shell. Figure 5 shows the deformations at loading stages A and B. Deformations appear around both hoop edges. Up to loading stage A, deformations appear only around both hoop edges as shown in Figure 5.

After loading stage A, deformation mode of the shell changes. The deformation at loading stage B is also presented in Figure 5.

4.1.2 *R/C shell under lateral concentrate load*

Figure 6 shows the load deformation relation under lateral concentrate load applied at the center of the shell.

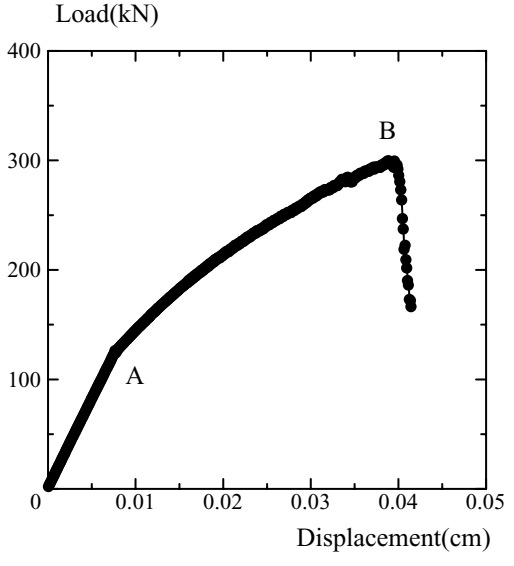

Figure 4. Axial load–displacement relation.

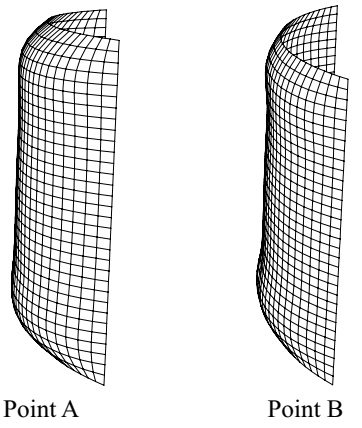

Figure 5. Deformation under axial compression.

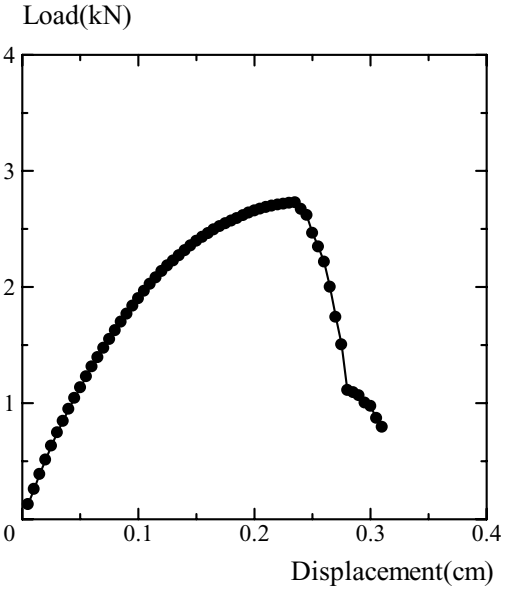

Figure 6. Lateral concentrate load–displacement relation.

R/C shell is pin-supported at both hoop and meridional edges. Targeted displacement point is the same as the loading point. The deformation is in the direction perpendicular to the shell plane.

Figure 7 represents the deformation mode under concentrate lateral load at the center. Large deformations appear around at the center of the shell. The deformation is the local phenomena along the meridional direction. R/C cylindrical shell surface deforms one and a half wave deformation in the hoop direction.

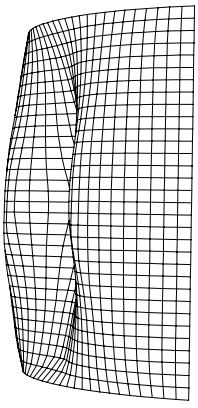

Figure 7. Deformation under lateral concentrate load.

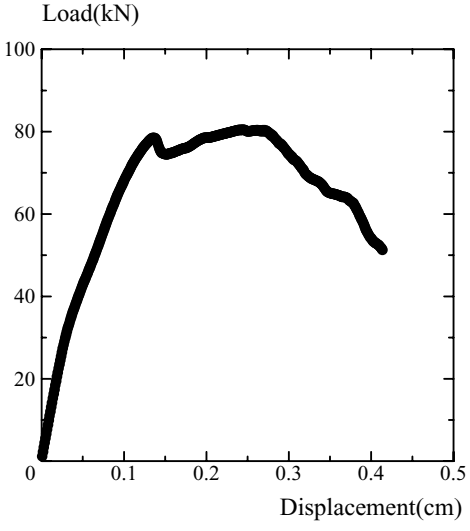

Figure 8. Lateral uniformly distribute load–displacement relation.

4.2 *R/C shell under lateral distribute load*

Figure 8 shows the load-deformation relation under the lateral uniformly distribute load. Uniformly distribute load is applied as the series of concentrate load mentioned in the previous chapter. R/C shell is pin-supported at both hoop and meridional edges. The displacement in the direction perpendicular to the shell plane is evaluated at the center of the shell surface. Figure 9 represents the deformation mode under lateral uniformly distribute load. Large deformations appear along the central meridian of the shell. R/C cylindrical shell surface also deforms one and a half wave deformation in the hoop direction. Total deformation is the same as that under concentrate loading. However,

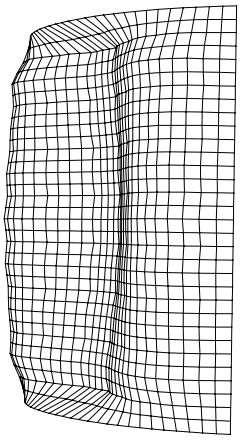

Figure 9. Deformation under lateral uniformly distribute load.

around the both hoop edges, there are steep deformations and the lateral load plays the predominant role for R/C shell deformation under the distribute loading.

4.3 *R/C shell under combined axial force and lateral concentrate load*

To investigate the deformation characteristics and the ultimate strength of R/C shell under combined axial and lateral loadings, parametric study is performed. Figure 10 shows the relation between lateral concentrate load and deformation in the direction perpendicular to the shell plane at the center of the shell after applying the axial loadings. The applied axial load is the 20% of the ultimate strength represented in Figure 4. Figure 11 shows the total deformation. The deformation pattern is the same as that only under concentrate loading (see Figure 7). Therefore, the effect of the axial loading concerning the combined loading effect is small.

To define the influences of the axial loadings into the ultimate strength under combined axial and lateral concentrate loadings, the ultimate strength is computed by use of the several axial loading levels as the parameter.

Figure 12 shows the load-deformation relation under combined loading condition. Applied axial loadings are 10%, 30% and 50% of the ultimate axial loading. From Figure 12, the larger the applied axial loading level is, the smaller the ultimate lateral loadings. However, the ultimate deformation is larger with increasing the axial loading level.

Figure 13 shows the relation between the ultimate strength and the applied axial compressive loading level under combined axial and lateral concentrate loadings. Figure shows the same tendencies as shown

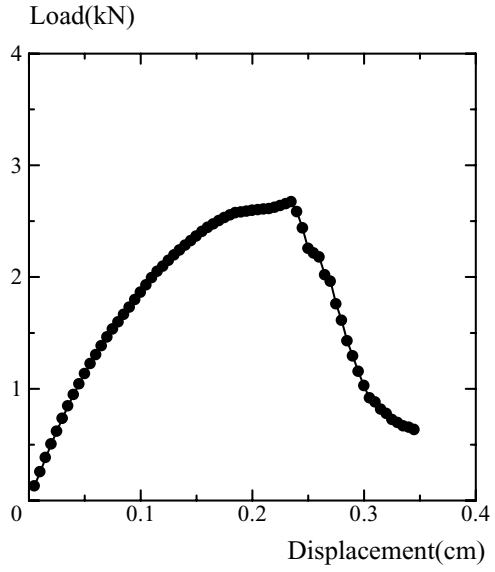

Figure 10. Relation between combined 20% of axial ultimate load and lateral concentrate load–displacement at center.

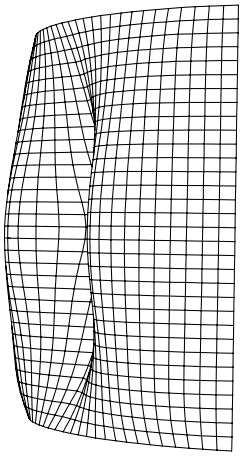

Figure 11. Deformation under combined 20% axial ultimate load and concentrate load.

in Figure 12. The applied axial force plays an important role for the ultimate strength of the shell under combined axial and lateral concentrate loadings.

4.3.1 *R/C shell under combined axial force and lateral uniformly distribute load*

Figure 14 shows the relation between lateral uniformly distribute load and deformation in the direction perpendicular to the shell plane at the center of the shell

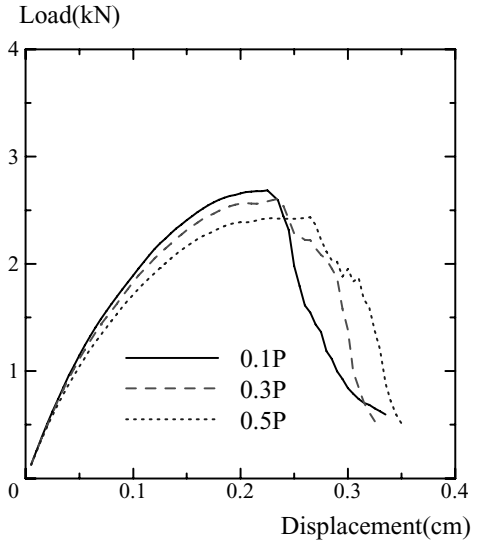

Figure 12. Load deformation relation of R/C shell under combined axial and lateral concentrate loadings.

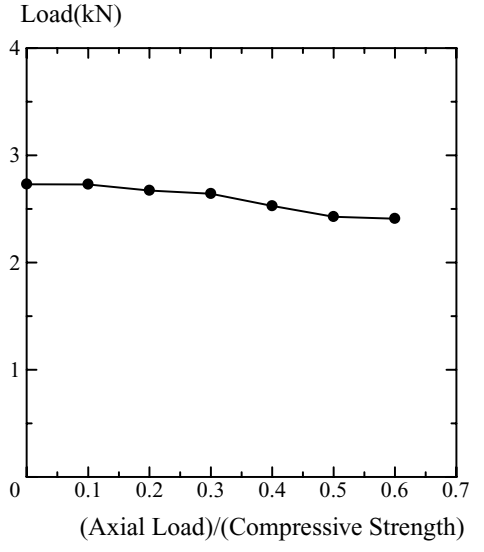

Figure 13. Ultimate load and the applied axial compressive load level under combined axial and lateral concentrate loadings.

after applying the axial loadings. The ordinate shows the total applied loading intensity to R/C shell surface. The applied axial load is also the 20% of the ultimate load represented in Figure 4. The ultimate strength under combined loading is larger than that under only lateral distribute loading.

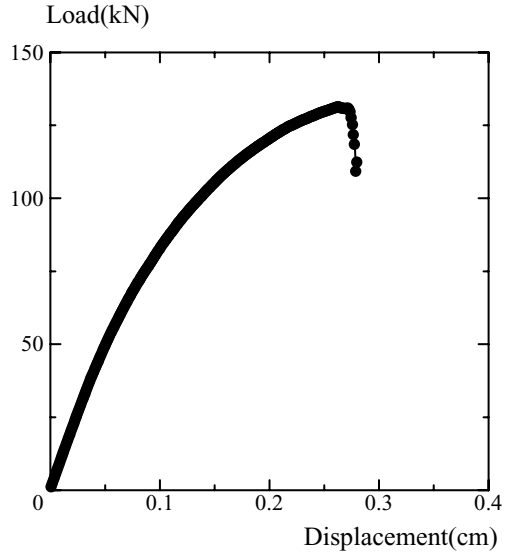

Figure 14. Relation between combined 20% of axial ultimate load and lateral uniformly distribute load–displacement at center.

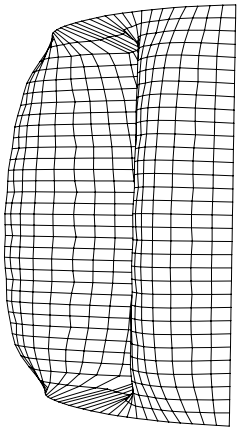

Figure 15. Deformation under combined 20% axial ultimate load and uniformly distribute load.

Figure 14 shows the total deformation. The deformation pattern is also the same as that only under uniformly distribute loading (see Figure 9). From the deformation analysis shown in Figure 5 under axial loading, R/C shell shows the convex deformation in upward.

Consequently, R/C shell deforms to the bidirectional convex configuration. In such case, R/C shell represents the high ultimate strength under lateral uniformly distribute load. Therefore, the ultimate strength

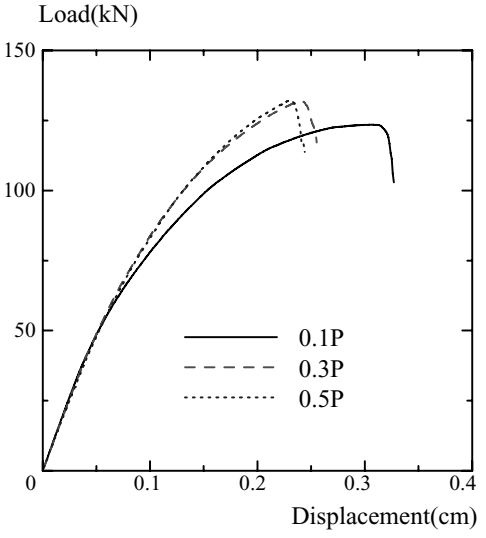

Figure 16. Load deformation relation of R/C shell under combined axial and lateral distribute loadings.

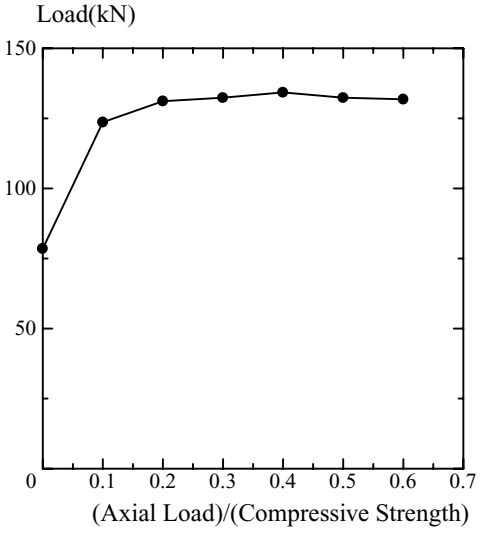

Figure 17. Ultimate load and the applied axial compressive load level under combined axial and lateral distribute loadings.

increases comparing with that only under laterally distribute load. The effect of the axial load concerning the combined loading effect is large under lateral uniformly distribute load.

To define the influences of the axial loadings into the ultimate strength under combined axial and lateral uniformly distribute loadings, the ultimate strength is

also computed under the same conditions as Figure 12. Figure 16 shows the load-deformation relation under combined axial and uniformly distribute loadings. Applied axial loadings are 10%, 30% and 50% of the ultimate axial loadings. The ultimate strength grows with the axial compressive load level. From Figure 16, the different results from that under combined axial and concentrate loadings are obtained. The larger the applied axial loading level is, the larger the ultimate lateral loading is. Also, the ultimate deformation is smaller with increasing the axial loading level. Figure 17 shows the relation between the ultimate strength and the applied axial compressive loading level under combined axial and lateral uniformly distribute loadings. From Figure 17, the increasing rate of the ultimate strength is small if the applied axial compression level exceeds 20% of axial ultimate load. Consequently, the applied axial force plays a predominate role for the ultimate strength of the shell under combined axial and lateral distribute loadings.

5 CONCLUSIONS

In this paper, the deformation characteristics and the ultimate strength of R/C cylindrical panel subjected to a combined axial and a flexural loadings are investigated numerically under the same geometric and supporting conditions as the previous researches.

From the parametric investigations, following conclusions are obtained.

1. The deformation of R/C shell under concentrate loading contributes to the local deformation around the applied load.
2. The deformation of R/C shell under distribute loading contributes to the global deformation on the shell surface.
3. The larger the axial compressive load is, the smaller the ultimate strength of R/C shell is when the combined axial and concentrate lateral loadings are applied.
4. The larger the axial compressive load is, he larger the ultimate strength of R/C shell is when the combined axial and lateral distribute loadings are applied. However, the effect of axial load is almost the same if the axial load level exceeds 20% of the ultimate compressive strength.

REFERENCES

Hara, T. 2008. Numerical and experimental evaluation of R/C shell. Proceedings of International Conference on Advances in Structural Engineering and Mechanics, 133–144.

Hinton, E. and Owen, D.J.R., 1984, Finite element software for plates and shells, Prineridge Press, Swansea, UK.

Kupfer, H. and Hilsdorf, K.H., 1969, Behavior of concrete under biaxial stress, ACI Journal 66(8) 656–666.